Biosensors and Bioelectronics 127 (2019) 118–125

Contents lists available at ScienceDirect

Biosensors and Bioelectronics

journal homepage: www.elsevier.com/locate/bios

Peptide-modified electrolyte-gated organic field effect transistor. Application to Cu^{2+} detection

T.T.K. Nguyen[a,b], H.V. Tran[c], T.T. Vu[b], S. Reisberg[a], V. Noël[a], G. Mattana[a], M.C. Pham[a], B. Piro[a,*]

[a] Univ. Paris Diderot, Sorbonne Paris Cité, ITODYS, UMR 7086 CNRS, 15 rue J-A de Baïf, 75205 Paris Cedex 13, France
[b] Department of Advanced Materials Science and Nanotechnology (AMSN), University of Science and Technology of Hanoi (USTH), Vietnam Academy of Science and Technology (VAST), 18 Hoang Quoc Viet, Nghĩa Đô, Cầu Giấy, Hanoi, Viet Nam
[c] Department of Inorganic Chemistry, School of Chemical Engineering, Hanoi University of Science and Technology (HUST), 1st Dai Co Viet Road, Hanoi, Viet Nam

ARTICLE INFO

Keywords:
Electrolyte-Gated Organic Field Effect Transistor
Peptide sensor
Cu^{2+} detection

ABSTRACT

This work proposes an approach for Cu^{2+} sensing in water which combines the selectivity of the Gly-Gly-His (GGH) peptide probe with the sensitivity of the electrolyte-gated organic field-effect transistor (EGOFET). The oligopeptide probe was immobilized onto the gate electrode of the transistor by electrooxidation of the primary amine of the glycine moiety. Cu^{2+} complexation by the grafted GGH was at first electrochemically evidenced, using cyclic and square wave voltammetries, then it was demonstrated that GGH-functionalized EGOFETs can transduce Cu^{2+} complexation through a significant threshold voltage shift and therefore a change in drain current. The limit of detection is ca. 10^{-12} M and the sensitivity in the linear range (10^{-12} – 10^{-8} M) is 1 mA dec^{-1} (drain current variations).

1. Introduction

Electrolyte-Gated Organic Field Effect Transistors (EGOFETs), also named Liquid-Gated OFETs (LG-OFETs), are very promising sensing devices. They are thin-film transistors (TFTs) based on organic semiconductors (OSC) where the non-electronically conducting material in-between the gate and the OSC is an electrolyte (Taniguchi and Kawai, 2004; Bäcklund et al., 2004; Panzer and Frisbie, 2006), such as aqueous biological buffers or even simple deionized water (Kergoat et al., 2010). The electrical behavior of EGOFETs in saturation regime can be described, in terms of current-voltage curves, by the quadratic equation commonly used for both inorganic and organic FETs (Eq. (1)).

$$I_{D,Sat} = \mu \frac{W}{2L} C_{Tot} (V_{GS} - V_{Th})^2 \quad (1)$$

In this equation, $I_{D,Sat}$ represents the drain current, W and L the channel width and length, respectively, V_{GS} the voltage difference between the gate electrode (V_G) and the source electrode (V_S), V_{Th} the threshold voltage, μ the charge carriers' mobility and C_{Tot} the total interfacial capacitance. One should note that, when Eq. (1) is applied to EGOFETs, the capacitive term C_{Tot} corresponds to the total capacitance between the gate electrode and the organic semiconductor and is composed of two different contributions, namely the capacitance associated to the gate/electrolyte interface and that corresponding to the electrolyte/semiconductor interface.

Under operation, for p-type semiconductors, the gate electrode is negatively polarized as well as the drain electrode, while the source is grounded. As a result, two electrical double layers (EDL) are formed at the gate/electrolyte and semiconductor/electrolyte interfaces and mirror charges (holes) accumulate within the OSC, forming the conductive channel. The density of charge carriers in the channel is directly dependent on the gate potential or, more precisely, on the density of charge at the respective interfaces. For a water/gold interface, for example, the capacitance is of several tens of μF cm^{-2}, i.e. a hundred times more than that of a classical dielectric/semiconductor interface (Porrazzo et al., 2014). Consequently, instead of the tens of volt that are necessary for operating classical solid-state dielectric-based OFETs, EGOFETs can be operated at hundred times lower voltages, i.e. a few hundreds of mV (Kergoat et al., 2012b).

Since the first description of EGOFETs operating in water (Kergoat et al., 2012a), EGOFET-based biosensors have been developing fast. Two different possible approaches can be used to obtain EGOFET-based biosensors, depending on where biofunctionalization occurs: at the semiconductor/electrolyte interface (Cotrone et al., 2012; Kergoat

* Corresponding author.
E-mail addresses: nguyenthithuykhue@gmail.com (T.T.K. Nguyen), hoang.tranvinh@hust.edu.vn (H.V. Tran), vu-thi.thu@usth.edu.vn (T.T. Vu), steeve.reisberg@univ-paris-diderot.fr (S. Reisberg), vincent.noel@univ-paris-diderot.fr (V. Noël), giorgio.mattana@univ-paris-diderot.fr (G. Mattana), mcpham@univ-paris-diderot.fr (M.C. Pham), piro@univ-paris-diderot.fr (B. Piro).

https://doi.org/10.1016/j.bios.2018.12.005
Received 22 October 2018; Received in revised form 5 December 2018; Accepted 6 December 2018
Available online 15 December 2018
0956-5663/

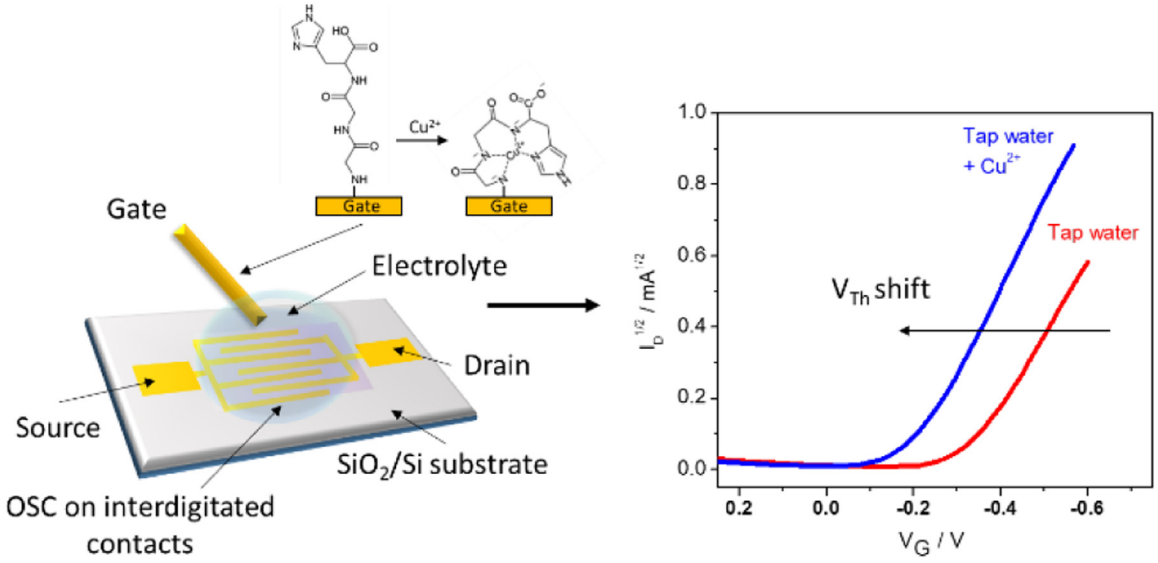

Fig. 1. Schematic representation of the electrolyte-gated organic field-effect transistor with spin-coated DPP-DTT semiconductor on top of interdigitated source and drain contacts, tap water as electrolyte and a gold gate onto which GGH is grafted. In the presence of Cu^{2+}, GGH folds, which modifies the gate/electrolyte interface and leads to a positive shift in threshold voltage.

et al., 2012b; Suspène et al., 2013; Palazzo et al., 2015; Magliulo et al., 2016; Piro et al., 2017), or at the gate/electrolyte interface (Casalini et al., 2013, 2015; Mulla et al., 2015; Berto et al., 2016; Diacci et al., 2017; Thomas et al., 2018; Nguyen et al., 2018; Fillaud et al., 2018; Berto et al., 2018).

However, analyte detection based on binding a target on a probe can be obtained only if the probe is sufficiently small not to screen the target from the gate electrode surface or undergoes a thorough structural reorganization upon binding; on this basis, gate-modified EGOFET immunosensors have been developed (Nguyen et al., 2018). Instead of antibodies, DNA can also be used as capture probes; for example, DNA-based EGOFETs have been described for hybridization of nucleic acids targets (White et al., 2015). Following the same idea, peptide aptamers, which have been thoroughly reported in electrochemical sensing devices or even in classical FETs, may also be used. Compared to the 4 nucleobases that code DNA, peptides are made of more than 20 amino acids, which considerably increases the number of possible ligand combinations (4^n versus 20^n, with n the number of nucleobases or amino acids in the sequence, respectively). However, this has been described only recently on EGOFETs, by Berto et al. (2018), who reported on a peptide aptasensor for the detection of tumor necrosis factor alpha (TNFα), a large protein of 25 kD. Peptides can also act as very effective and specific capture probes for metal ions (Sigel and Martin, 1982; Kozlowski et al., 1999). To illustrate these properties in view of electrochemical detection, Gooding and colleagues used the copper binding tripeptide Gly-Gly-His (glycine-glycine-histidine) for detecting Cu^{2+} in aqueous media and published a series of articles on this topic (Yang et al., 2001, 2003; Gooding et al., 2001; Chow and Gooding, 2006; Wawrzyniak et al., 2013).

From an analytical point of view, copper is a transition metal essential for life. At elevated concentrations, however, it is toxic to organisms such as algae, fungi, and many bacteria, and in humans may adversely affect the gastrointestinal, hepatic, and renal systems. It should be stressed that the innocuity of copper in drinking water at concentrations below 2 mg L^{-1}, corresponding to the values proposed by the World Health Organization in 1993 (WHO, 1993), has been questioned several times since. For these reasons, it is pertinent to develop a sensitive method for on-site determination of free Cu^{2+} ions in aqueous media. Of course, copper can be detected and quantified by routine methods, including the most common one (flame atomic absorption spectrometry; limit of detection -LoD- in the µg L^{-1} range, i.e. more than 10 nM), the most sensitive one (mass spectrometry coupled to inductively coupled plasma; LoD of 5 ng L^{-1}), or by methods more adapted to a point-of-use format such as optical (Liu and Lu, 2007; Xu et al., 2010; Yao et al., 2013; Udhayakumari et al., 2017) or electrochemical techniques (Wawrzyniak et al., 2013; Gan et al., 2016; Zhu et al., 2017 or other references of Gooding and coworkers already cited above).

Unlike optical devices, EGOFETs operate at very low voltage, integrate no fragile elements (light source, photodetector) and provide analogic output signals directly usable by an electronic controller. Furthermore, compared to electrochemical transducers, EGOFETs do not require the use of a reference electrode (which simplifies the fabrication process) and, more importantly, are able to characterize a broader set of physicochemical phenomena, including processes that do not involve faradic processes. Also, the surface of these devices may be small (a fraction of mm^2) and their size can be decreased down to the limits afforded by microlithography, which permits decreasing the electrolyte volume accordingly and eventually use microfluidic cells. Photolithography allowing mass fabrication, the unit cost of an EGOFET is low, which makes it disposable. Other fabrication procedures, such as inkjet printing, will, in the near future, decrease even more their production cost. There is therefore a major interest in extending the development of EGOFETs in the biosensors field.

In this work, we propose for the first time an approach which combines the selectivity of the Gly-Gly-His peptide probe (GGH) with the sensitivity of EGOFETs, in particular using the gate-functionalization strategy, where the peptide was immobilized by direct electrooxidation of the primary amine of the first glycine moiety of GGH. Cu^{2+} complexation by grafted GGH was first evidenced electrochemically, using cyclic and square wave voltammetries, then it was demonstrated that GGH-modified EGOFETs can transduce Cu^{2+} complexation through variations of the EGOFETs output and transfer curves. In particular, the threshold voltage (V_{Th}) shift was identified as a good quantitative parameter. Fig. 1 summarizes the approach followed in this work.

2. Materials and methods

2.1. Chemicals and materials

The fabrication procedures for the lithographied transistors and the gate microelectrodes are described in Sections SI.1 and SI.2 of the

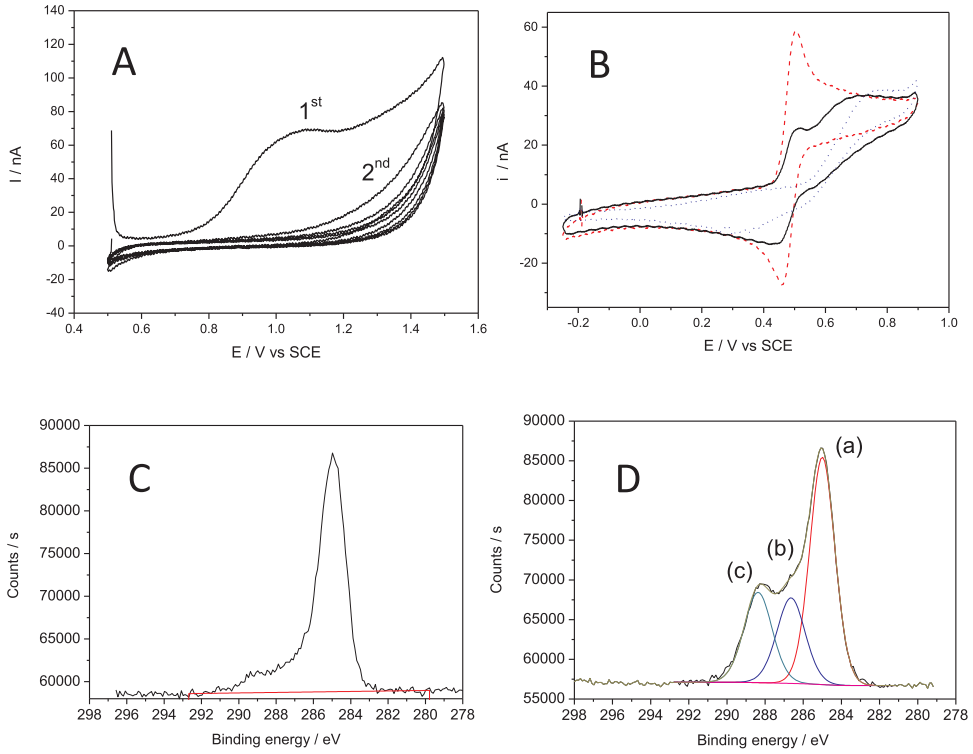

Fig. 2. (A) Cyclic voltammograms (5 cycles, v = 50 mV s^{-1}, between 0.5 V and 1.5 V) corresponding to electrooxidation of Gly-Gly-His (5 mM) on a gold gate (diameter = 100 µm), in argon-saturated PBS. The first cycle shows an oxidation wave corresponding to the oxidation of the primary amine of the first Gly residue. Following cycles show partial passivation. **(B)** Cyclic voltammograms recorded in 0.1 M H_2SO_4 + 10^{-3} M dopamine with a 100 µm bare gold gate electrode (red dashed curve), the same electrode modified with GGH as described above (black solid curve) and the same electrode modified with GGH + 3-MCP (blue dotted curve). **(C)** XPS spectrum of C_{1s} for a bare gold gate electrode and **(D)** XPS spectrum of C_{1s} for a GGH-modified gold gate electrode. (For interpretation of the references to color in this figure legend, the reader is referred to the web version of this article).

Supplementary information document, respectively. Gly-Gly-His (diglycyl-histidine, CAS Number 7451-76-5) was purchased from Sigma-Aldrich. Poly(N-alkyldiketopyrrolopyrrole dithienylthieno[3,2-b]thiophene) (DPP-DTT) was purchased from Ossila (England), with M_w = 280 ± 10 kDa and PDI = 3.8 ± 0.1. Lithium perchlorate ($LiClO_4$) 98% was purchased from Alfa Aesar. Copper(II) sulfate pentahydrate ($CuSO_4{\cdot}5H_2O$) was purchased from Prolabo, France. Phosphate buffer saline (PBS), dichlorobenzene 98%, chlorobenzene - anhydrous, 99.8%, isopropanol, 3-mercapto propanol (3-MCP) and all other reagents and solvents were purchased from Sigma Aldrich and used without further purification. Aqueous solutions were made with MilliQ water or tap water, depending on conditions.

2.2. Gate functionalization

Gly-Gly-His peptide was grafted on 100 µm diameter homemade gold microelectrodes by sweeping the electrode, in MilliQ water containing 5 mM Gly-Gly-His + 0.1 M $LiClO_4$ as supporting electrolyte, between + 0.5 V and + 1.5 V at 50 mV s^{-1} for five cycles.

2.3. X-ray photoelectron spectroscopy characterizations

For XPS characterization, 1 cm^2 pieces of gold-coated silicon wafers were used instead of gold microelectrodes. The spectrometer was a Thermo ESCALAB using a monochromic Al Kα source at 1486.6 eV.

2.4. Electrochemical and electrical characterizations

Electrografting of the Gly-Gly-His peptide was characterized using dopamine as redox probe. Cyclic voltammetry and square wave voltammetry were performed on an Autolab PGSTAT 302 N controlled by NOVA 2.0 software. A conventional three-electrode setup was used, with a platinum grid of about 2 cm^2 as counter electrode, a commercial saturated calomel reference electrode (SCE, Metrohm) used through a salt bridge, and home-made glass-sealed Au microelectrodes as working electrodes (100 µm in diameter). Square wave voltammetry (SWV) was performed using a modulation amplitude of 50 mV, an interval time of 80 ms, a step of 2 mV and a frequency of 12.5 Hz. Electrochemical impedance spectroscopy (EIS) was performed with the same equipment and cell. The frequency ranged from 100 kHz to 100 mHz, with a perturbation amplitude of 10 mV. An equivalent circuit composed of a resistance R_E (electrode + electrolyte resistance) in series with a parallel $R_{DL}C_{DL}$ circuit (resistance and capacitance of the electrical double layer) was used for fitting.

For the measurement of the transistors characteristics, a lab-made PDMS cover forming a well (3 mm in diameter, 5 mm in depth) was put over the semiconducting channel and filled with 200 µL of solution (PBS or MilliQ water), into which the gate electrode was dipped. Output characteristics were recorded by sweeping the drain-source voltage between 0 V and − 0.40 V at 170 mV s^{-1}; the gate voltage V_{GS} was incrementally switched from + 0.3 V to − 0.6 V by steps of 0.1 V. The off current (I_{off}) corresponds to V_{GS} = 0 V and the on current (I_{on}) to V_{GS} = -0.6 V. Transfer curves were obtained by sweeping V_{GS} from 0.2 V to − 0.6 V at 170 mV s^{-1} at constant V_{DS} = -0.4 V. The electrical characteristics were recorded using a Keithley 4200 Semiconductor Characterization System.

3. Results and discussion

3.1. Grafting of the Gly-Gly-His peptide probe

There are multiple examples of peptide immobilization on electrodes available in the literature. Among the reported techniques, the two approaches which have been already employed for functionalization of EGOFETs gates are self-assembly of alkylthiols on gold (Casalini et al., 2013, 2015; Mulla et al., 2015; Berto et al., 2016; Diacci et al., 2017; Thomas et al., 2018) and, more recently, aryl diazonium electrografting (Nguyen et al., 2018; Fillaud et al., 2018). However, these approaches may imply that the active part of the capture probe is separated from the gate surface by the anchoring moiety (alkylthiol chain or aryl diazonium group). However, the sensitivity of EGOFETs is best when the capture probe is immobilized as close as possible to the gate metallic surface; for this reason, Berto et al. (2018) proposed the direct immobilization of a histidine-tagged Affimer on the gate electrode of an

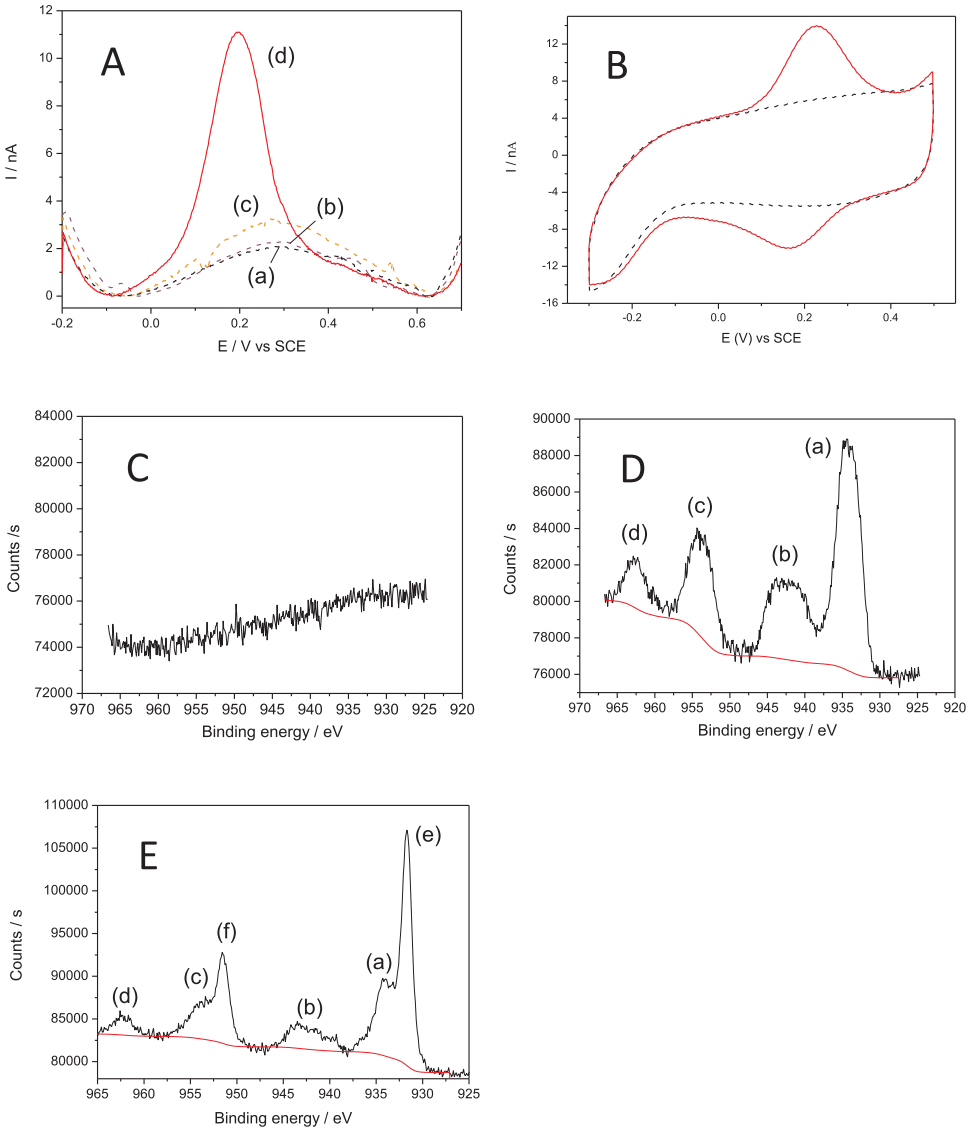

Fig. 3. (A) Square wave voltammograms of (a, black) a GGH-modified gate electrode (diameter = 100 µm) in PBS; (b, purple) GGH-modified gate electrode incubated in 10^{-5} M $MnCl_2$; (c, orange) GGH-modified gate electrode incubated in 10^{-5} M $FeSO_4$; (d, red) GGH-modified gate electrode incubated in 10^{-5} M $CuSO_4$. **(B)** CVs of a GGH-modified gate electrode in PBS (black dashed curve) and after incubation in 10^{-5} M $CuSO_4$ (red curve); scan rate 100 mV s^{-1}. **(C)** XPS spectrum, in the copper region, of a bare Au gate incubated in 10^{-5} M $CuSO_4$; **(D)** XPS spectrum of a Cu^{2+}@GGH-modified Au gate incubated in 10^{-5} M $CuSO_4$ then used as gate electrode in transistor configuration. **(E)** XPS spectrum of a Cu^{2+}@GGH-modified Au gate incubated in 10^{-5} M $CuSO_4$ then polarized in PBS at −0.1 V vs SCE to reduced Cu^{2+} into Cu(0). (For interpretation of the references to color in this figure legend, the reader is referred to the web version of this article).

EGOFET, instead of employing conventional antibodies (Affimers are commercial 12–14 kDa proteins significantly smaller than IgG antibodies) and reported excellent results.

In this work, we were guided by a similar idea. We propose here the direct electrografting of the Gly-Gly-His peptide through the first primary amine-terminated Gly residue. Barbier et al. (1990), then Deinhammer et al. (1994), Bélanger and Pinson (2011). Fig. 2**A** shows CVs obtained for electrografting of 5 mM GGH in PBS. The first scan highlights glycine oxidation, starting at ca. 0.7 V vs SCE. Further cycling shows progressive passivation of the electrode (the oxidation starts at ca. 1 V during the second scan and can be considered negligible for the following cycles). Fig. 2**B** shows CVs characterizing the electrode state before (red dashed curve) and after (black curve) GGH grafting for 5 cycles, using dopamine as redox probe. As shown, dopamine still reacts after grafting, through a mixed process which shows that the surface is not completely blocked. A better blocking was achieved after adsorption of 3-mercaptopropanol on a GGH-grafted electrode (GGH-modified electrodes were put in a 10^{-5} M aqueous 3-MCP solution for 2 h; blue dotted curve). However, electron transfer still takes place, probably across the thin peptide monolayer.

XPS was performed on bare and GGH-modified electrodes (Fig. 2**C,D**) to characterize GGH grafting (XPS data are gathered in Table SI.1). The C_{1s} spectrum of the bare gold electrode shows the usual carbon contamination, with a main peak at 285 eV corresponding to C-C and C=C aliphatic carbons and a small proportion (4%) of C-O and O-C=O carbons around 289 eV. Conversely, the C_{1s} spectrum of the GGH-modified gold electrode shows three peaks at 285 (a), 286.6 (b) and 288.4 (c) eV. The GGH peptide (chemical structure shown on Fig. 1) carries 10 carbons, of which only one is purely aliphatic and bound to other carbon atoms (C-C or C=C); it is expected to appear at 285 eV. Considering that the C_{1s} spectrum of the unmodified Au gate shows aliphatic C-C or C=C carbons with a similar intensity to the one observed for the GGH-modified gate, the contribution of this unique carbon from GGH at 285 eV was not considered. 5 other carbons (C-N) from GGH are expected to appear at 286.6 eV and 4 carbons (C-O, C=N, C=O and O-C=O) at 288.4 eV. For a quantitative analysis, we considered only carbons from C-N, C-O, C=N, C=O and O-C=O, and nitrogen N_{1s} (other atoms such as C-C, C=C or O_{1s} were present on bare gold and considered as surface pollutants). The ratios given on the last column of Table SI.1 are consistent with the actual atomic ratio, theoretical 33% for C-N (actual measured value: 29.7%), theoretical 26.7% for C=N, C= 0 and O-C=O (actual measured value: 31.5%) and theoretical 33% for N_{1s} (actual measured value: 38.8%). The excess of nitrogen partly comes from polluting nitrogen, which represents ca. 10% of the total nitrogen, as measured on the non-modified Au surface.

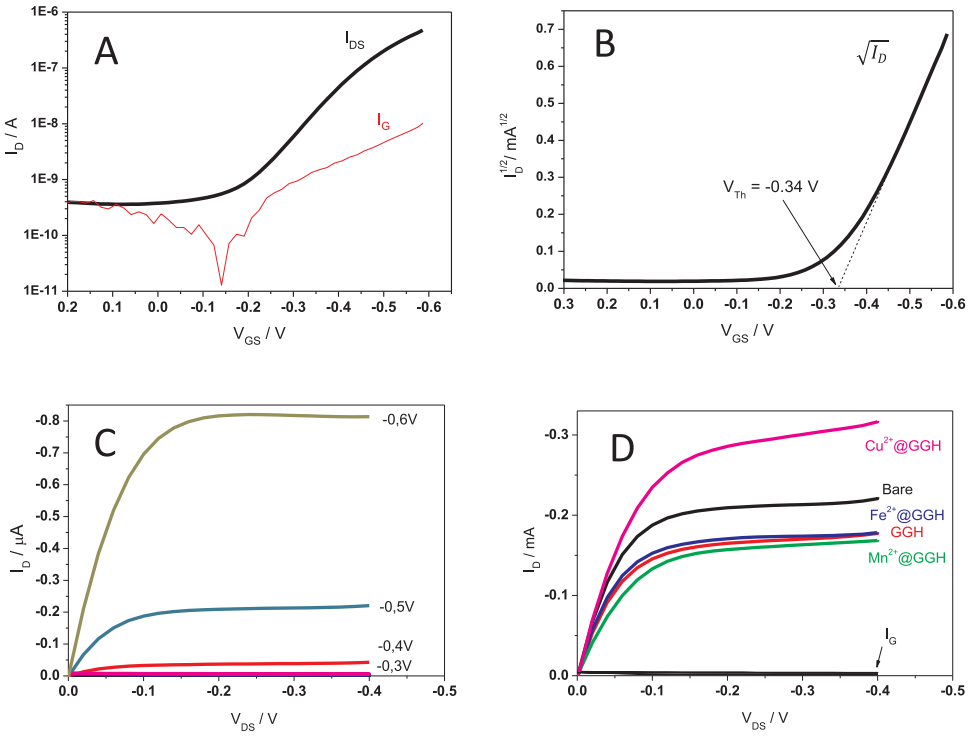

Fig. 4. (A) Transfer curve (black) of a bare Au gate EGOFET obtained by sweeping the gate voltage form + 0.2 V down to −0.6 V. Scan rate of 170 mV s^{-1}; V_{DS} = -0.4 V. Gate current shown in red. **(B)** Corresponding plot of $\sqrt{I_D}$ = f(V_{GS}) (black). L = 10 µm; W = 10 mm. Electrolyte: aerated MilliQ water. **(C)** Output curves at various gate voltages, for a bare Au gate. **(D)** Output curves (V_{GS} = −0.5 V) for bare Au gate, GGH-modified gate and for GGH-modified gates incubated in 10^{-5} M Fe^{2+}, Mn^{2+} or Cu^{2+}. (For interpretation of the references to color in this figure legend, the reader is referred to the web version of this article).

3.2. Characterization of Cu^{2+} capture

To characterize Cu^{2+} capture by the GGH layer, square wave voltammetry (SWV) was performed on GGH-modified gate electrodes after incubation in PBS, PBS + 10^{-5} M $MnCl_2$, PBS + 10^{-5} M $FeSO_4$ and PBS + 10^{-5} M $CuSO_4$ (Fig. 3**A**). It appears that no change in current was observed for electrodes incubated in Mn^{2+}, and only a small change for electrodes incubated in Fe^{2+}. Conversely, an intense peak current was observed for the electrode incubated in Cu^{2+}, corresponding to the Cu (II)/Cu(0) redox couple (Wawrzyniak et al., 2013). Cyclic voltammetry was performed on GGH-modified gate electrodes after incubation in PBS and PBS + 10^{-5} M $CuSO_4$ (Fig. 3**B**). Peak currents were shown to vary linearly with the scan rate between 10 and 200 mV s^{-1} (not shown), which demonstrates that the process is not diffusion-limited and confirms that the electroactive copper comes from the GGH layer at the extreme vicinity of the electrode. A similar behavior was observed by Yang et al. (2003). Integration of the oxidation and reduction peaks, assuming a two-electron process, gave a coulombic charge of $Q_{Cu2+,ox}$ = 24 nC and $Q_{Cu2+,ox}$ = 20 nC, i.e. a surface concentration of accessible Cu^{2+} of Γ_{Cu2+} = 1.3–1.6 × 10^{-9} mol cm^{-2}, which is consistent with the density of a GGH monolayer on a gold electrode and with other reported values for similar systems (Liu et al., 2006; Wawrzyniak et al., 2013).

XPS was performed on a non-modified Au electrode after incubation in a solution containing Cu^{2+} (Fig. 3**C**) and compared to a GGH-modified Au electrode after incubation in the same conditions then used as gate in a transistor (noted Cu^{2+}@GGH-modified gate). On the bare Au gate, no copper is observed; on the contrary, on the Cu^{2+}@GGH-modified gate, four peaks are visible and all of them can be typically attributed to Cu(II): the strong spin-orbit split (ΔE = 19.8 eV, with an intensity ratio of 0.5) of $Cu_{2p1/2}$ at 934.2 eV **(c)** and $Cu_{2p3/2}$ at 954 eV **(a)**, along with the two strong typical Cu^{2+} satellites at 942.4 eV **(b)** and 962.8 eV **(d)** (the double peak at 942.4 eV is typical of Cu(II)). No Cu(0) is observed.

XPS was also performed on a Cu^{2+}@GGH-modified Au gate incubated in 10^{-5} M $CuSO_4$ then put back in PBS and polarized at a negative potential (−0.1 V vs SCE) in order to reduce Cu^{2+} ions into Cu (0). As shown on Fig. 3**E**, in addition to the four peaks identified on Fig. 3D, the two peaks corresponding to Cu(0) appear: one at 932 eV ($Cu_{2p3/2}$) **(e)** and the other at 951.8 eV ($Cu_{2p1/2}$) **(f)**. Differences between spectra D and E confirms that no Cu(0) is formed on the gate electrode under transistor operation.

3.3. Electrical characterizations

As discussed in the introduction, the electrical characteristics of EGOFETs for which the gate capacitance is significantly smaller than that of the channel (channel capacitance was found to be ca. 35 ± 15 nF for an active area of 0.5 mm^2, versus a gate capacitance varying between 2.7 and 4.2 nF) are mostly dependent on the gate/electrolyte interface (Nguyen et al., 2018). Fig. 4**A** shows the transfer curve of a bare Au-gated EGOFET and the corresponding gate current. The device shows a typical field-effect behavior, with a weak gate current 50 times lower than the drain current at V_{GS} = -0.5 V and a transconductance $g_{m,Au} = \frac{\partial I_D}{\partial V_G}$ of 3 µS at −0.5 V. Fig. 4**B** shows the corresponding $\sqrt{i_D}$ curve used to estimate the threshold voltage from the intercept in saturation regime; V_{Th} = -0.34 ± 0.01 V. Fig. 4**C** shows the output curves at different V_{GS} from + 0.2 V to −0.6 V (only curves from −0.3 V to −0.6 V are visible, curves from 0.2 to −0.2 V overlap). The I_{on}/I_{off} ratio is high, ca. 1200, which demonstrates the excellent quality of the device.

3.4. Characterization of Cu^{2+} capture in transistor configuration

On Fig. 4**D** are shown the output curves obtained with bare gate, GGH-modified gate and GGH- modified gates incubated with 10^{-5} M Cu^{2+}, Mn^{2+} or Fe^{2+}. Behaviors are consistent with capacitances shown in Section 3.2: I_D decreases after grafting of GGH but increases when

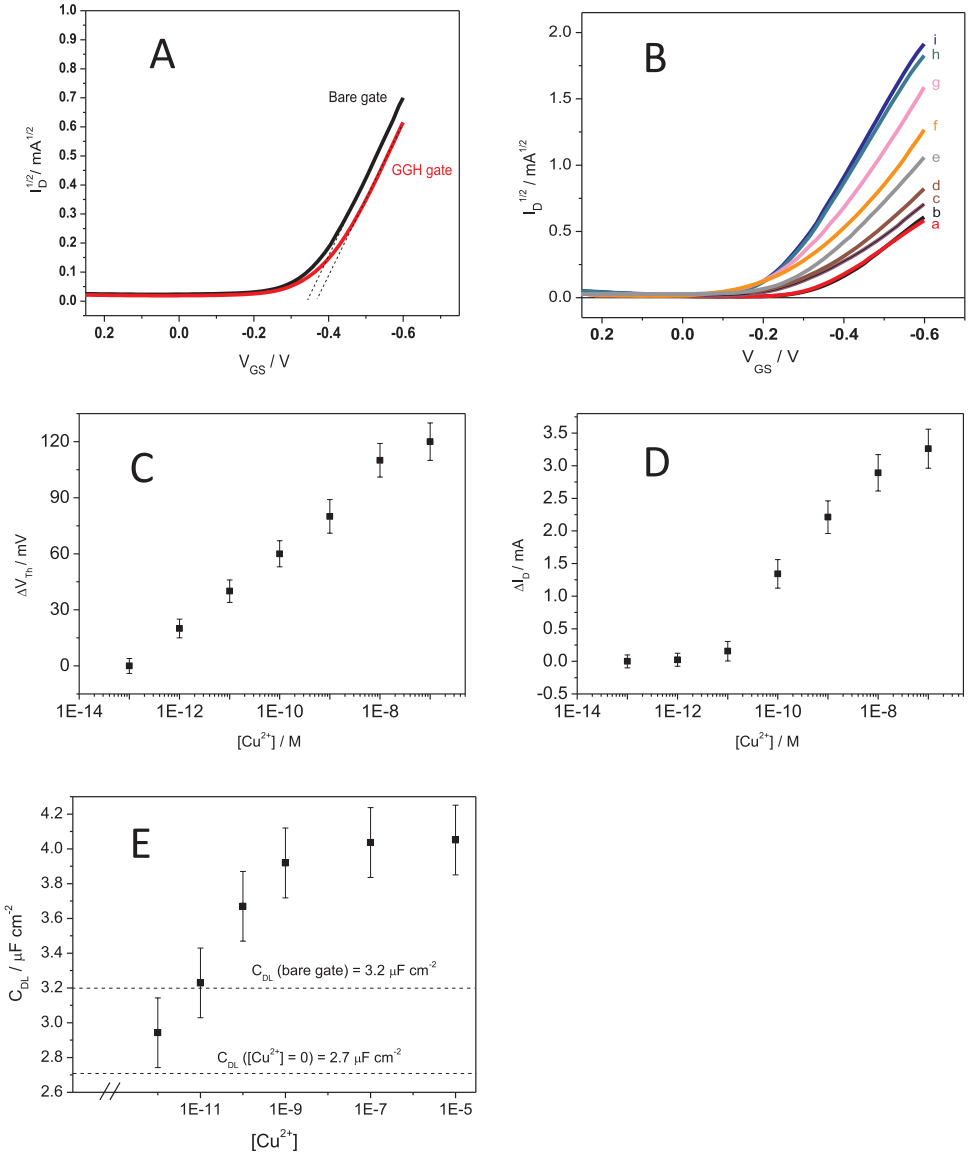

Fig. 5. (A) Plots of $\sqrt{I_D}$ = f(V_{GS}) for a bare Au gate (black) and GGH-modified gate (red); both experiments in aerated MilliQ water. V_{Th} (Bare/MilliQ) = -0.34 ± 0.01 V; V_{Th} (GGH/MilliQ) = -0.36 ± 0.01 V. **(B)** Plots of $\sqrt{I_D}$ = f(V_{GS}) for Cu^{2+}@GGH-modified gates in tap water for various Cu^{2+} concentrations (a: no Cu^{2+}; b: 10^{-13} M Cu^{2+}; c: 10^{-12} M; d: 10^{-11} M; e: 10^{-10} M; f: 5.10^{-10} M; g: 10^{-9} M; h: 10^{-8} M; i: 10^{-7} M.). V_{Th} (GGH/Tap water) = -0.34 ± 0.01 V. V_{Th} (Cu^{2+}@GGH/Tap water) = -0.22 ± 0.01 V for [Cu^{2+}] = 10^{-7} M. V_{DS} = -0.4 V. **(C)** Calibration curve obtained from variations in V_{Th} as a function of [Cu^{2+}]. ΔV_{Th} = V_{Th} (Cu^{2+}@GGH) - V_{Th} (GGH). **(D)** Calibration curve obtained from I_D variations (at V_{DS} = −0.4 V and V_{GS} = −0.6 V) as a function of [Cu^{2+}]. **(E)** Double-layer capacitances (C_{DL}) of Cu^{2+}@GGH-modified gates as a function of $CuSO_4$ concentration. The capacitance for the bare Au electrode and for a GGH-modified gate before complexation of Cu^{2+} are also given. Results obtained from 3 experiments. (For interpretation of the references to color in this figure legend, the reader is referred to the web version of this article).

Cu^{2+} is complexed. Fig. 5**A** shows the small shift in threshold voltage (V_{Th} = -0.36 ± 0.01 V; $\Delta V_{Th} \approx -0.02$ V) induced by the presence of GGH on the gate electrode. The maximum transconductance $g_{m,GGH}$ is ca. 2.0 µS at −0.5 V, i.e. lower than $g_{m,Au}$. Fig. 5**B** shows that the threshold voltage is significantly shifted upon Cu^{2+} uptake; ΔV_{Th} = (120 ± 20) mV for [Cu^{2+}] = 10^{-7} M.

The drain current flowing through EGOFET devices is known to be sensitive to several parameters: the threshold voltage V_{Th}, the total capacitance C_{Tot} and the charge carriers' mobility µ. The transconductance g_m (slope of the transfer curves) is proportional to the product of the latter two, $g_m = \frac{W}{L}\ \mu\ C_{Tot}$.

The gate electrode functionalization and its response to Cu^{2+} ions were characterized in terms of EIS (characterization of the gate/electrolyte capacitance). Measurements were performed at a constant potential of −0.1 V (minimal faradic current) and frequencies between 10^5 and 10^{-1} Hz on bare Au, on GGH-grafting and on Cu^{2+}@GGH-modified electrodes. The double layer capacitance was extracted by fitting the equivalent $R_E[R_{DL}C_{DL}]$ circuit in the high frequency region. The bare Au electrode showed a total capacitance of 3.2 nF, corresponding to a capacitance per unit area of 40 µF cm^{-2}. For the GGH-modified electrode before Cu^{2+} complexation, the capacitance decreased down to 2.7 nF (33.8 µF cm^{-2}), whereas it increased for Cu^{2+}@GGH-modified gate; saturation occurred for [Cu^{2+}] > 10^{-9} M (Fig. 5**E**).

Upon copper complexation by GGH, g_m increases: Cu^{2+}@GGH-modified gate devices present a $g_{m,\ Cu2+@GGH}$ = 28 µS at −0.5 V for 10^{-7} M Cu^{2+}, significantly higher than for GGH-modified gate without copper. This increase is much more pronounced than the capacitance increase shown on Fig. 3F, which indicates that the capacitance is not the only factor responsible for the current increase. Indeed, it is shown

that V_{Th} changes more significantly, strongly shifting towards more positive values (shift of ca. + 0.12 V for incubation in [Cu^{2+}] = 10^{-7} M).

We have shown by XPS measurements that no Cu(0) is formed at the gate under transistor operation. The positive shift may be explained in terms of charge distribution at the interfaces: accumulation of Cu^{2+} at the gate interface, for a given negative gate voltage, increases the amount of positive charges at this interface, so that less negative potential is needed to accumulate a given charge density at the gate and symmetrically a given holes density within the semiconductor. We observed the same behavior in a previous work (Fillaud et al., 2018) in which protonation of a hydrogel on the gate electrode led to a positive V_{Th} shift as well. A similar behavior of V_{Th} shift as a function of charges immobilized on the gate electrode has also been reported by other authors (Buth et al., 2011, 2012; Berto et al., 2018; Diacci et al., 2017; Macchia et al., 2018).

3.5. Cu^{2+} detection

In terms of analytical applications, we have shown that the transfer characteristics are poorly affected by the nature of the electrolyte, whether tap or MilliQ water, which allowed us to apply our device to the detection of Cu^{2+} cations in tap water. The tap water we used did not contain copper but contained iron (1.8 µg L^{-1}), free chlorine (0.2 mg L^{-1}), nitrates (27.7 mg L^{-1}), calcium (94.7 mg L^{-1}), dihydrogenocarbonates (250 mg L^{-1}), chloride (24.2 mg L^{-1}), fluoride (0.1 mg L^{-1}), potassium (2.1 mg L^{-1}), sodium (8.1 mg L^{-1}), sulfates (20.5 mg L^{-1}), for a conductivity of around 500 µS cm^{-1} (data: *Eau de Paris*, 13th district, April 2018). Therefore, Cu^{2+} ions were added into aerated tap water (pH 7.7) by injection of a variable volume of a copper sulfate solution, into which the 100 µm GGH-modified gold electrode was incubated during 15 min, then rinsed in tap water for 2 min. The Cu^{2+}@GGH-modified electrode was then used as gate for acquiring the electrical characteristics of the transistor. The same experiment was made for various Cu^{2+} concentrations and repeated at least three times for each concentration. Fig. 5**C** shows the calibration curve relative to ΔV_{Th}, with a linear variation of the threshold voltage versus log[Cu^{2+}] between 10^{-13} to 10^{-8} M (for higher concentrations, ΔV_{Th} starts to level off). The sensitivity extracted from the slope of ΔV_{Th} in its linear region is S_{Th} = 20 mV dec^{-1}. Fig. 5**D** shows the calibration curve relative to ΔI_D, for which a linear region is defined between 10^{-11} M and 10^{-8} M, with a sensitivity of S_{Id} = 1 mA dec^{-1}. Considering a S/N ratio of 3, the limit of detection (LoD) is ca. 5.10^{-11} M when considering drain current changes, and is significantly lower, ca. 5.10^{-13} M when considering threshold voltage changes. These LoD are comparable to other electrochemical sensors using the Gly-Gly-His peptide as probe (Yang et al., 2001, 2003; Gooding et al., 2001; Chow and Gooding, 2006; Wawrzyniak et al., 2013).

4. Conclusion

EGOFETs in which the gate electrode is modified with the tripeptide Gly-Gly-His can transduce Cu^{2+} complexation through a significant threshold voltage shift. Due to the intrinsic amplification capability of such kind of transistors, this voltage shift is amplified into a large drain current variation. This phenomenon has been reported in other works dealing with EGOFETs for which gates were modified with charged probes or targets, but never for ion sensing using a peptide probe. These results pave the way for the detection of any kind of ions through functionalization of the gate electrode with an adequate ionophore. We now plan to investigate how these EGOFETs can be implemented into a microfluidic cell, for continuous measurement under electrolyte flow. This will allow us to investigate the reuse of our devices, i.e. the recycling of the gate after complexation of Cu^{2+} by the peptide. We plan to explore these aspects as soon as we develop a microfluidic cell into which the EGOFET will be integrated. Not only will this allow the investigation of several different applications but it will also permit characterizing important fundamental aspects such as complexation thermodynamics and the kinetics of molecular recognitions. Differential measurement strategies, in which two or more transistors are measured at the same time, are also being developed to address the current drift issue, inherently present into organic transistors.

CRediT authorship contribution statement

T.T.K. Nguyen: Investigation, Data curation. **H.V. Tran:** Investigation, Methodology. **T.T. Vu:** Investigation. **S. Reisberg:** Conceptualization. **V. Noël:** Methodology, Writing - review & editing. **G. Mattana:** Writing - review & editing. **M.C. Pham:** Resources, Funding acquisition. **B. Piro:** Conceptualization, Methodology, Writing - original draft, Writing - review & editing, Visualization, Project administration, Funding acquisition.

Acknowledgments

ANR (Agence Nationale de la Recherche) and CGI (Commissariat à l'Investissement d'Avenir) are gratefully acknowledged for their financial support of this work through Labex SEAM (Science and Engineering for Advanced Materials and devices), ANR 11 LABX 086, ANR 11 IDEX 05 02. TTKN thanks USTH (University of Science and Technology of Hanoi), Vietnam, for providing a Ph.D. grant. HVT and TTV thanks University Paris Diderot, France, for an internship grant.

Appendix A. Supporting information

Supplementary data associated with this article can be found in the online version at doi:10.1016/j.bios.2018.12.005.

References

Bäcklund, T.G., Sandberg, H.G.O., Österbacka, R., Stubb, H., 2004. Appl. Phys. Lett. 85, 3887.
Barbier, B., Pinson, J., Desarmot, G., Sanchez, M., 1990. J. Electrochem. Soc. 137, 1757–1764.
Bélanger, D., Pinson, J., 2011. Chem. Soc. Rev. 40, 3995–4048.
Berto, M., Casalini, S., Di Lauro, M., Marasso, S.L., Cocuzza, M., Perrone, D., Pinti, M., Cossarizza, A., Pirri, C.F., Simon, D.T., Berggren, M., Zerbetto, F., Bortolotti, C.A., Biscarini, F., 2016. Anal. Chem. 88, 12330–12338.
Berto, M., Diacci, C., D'Agata, R., Pinti, M., Bianchini, E., Di Lauro, M., Casalini, S., Cossarizza, A., Berggren, M., Simon, D.T., Spoto, G., Biscarini, F., Bortolotti, C.A., 2018. Adv. Biosyst. 2, 1700072.
Buth, F., Donner, A., Sachsenhauser, M., Stutzmann, M., Garrido, J.A., 2012. Adv. Mater. 24, 4511–4517.
Buth, F., Kumar, D., Stutzmann, M., Garrido, J.A., 2011. Appl. Phys. Lett. 98, 153302.
Casalini, S., Dumitru, A.C., Leonardi, F., Bortolotti, C.A., Herruzo, E.T., Campana, A., De Oliveira, R.F., Cramer, T., Garcia, R., Biscarini, F., 2015. ACS Nano 9, 5051–5062.
Casalini, S., Leonardi, F., Cramer, T., Biscarini, F., 2013. Org. Electron. 14, 156–163.
Chow, E., Gooding, J., 2006. Electroanalysis 18, 1437–1448.
Cotrone, S., Ambrico, M., Toss, H., Angione, M.D., Magliulo, M., Mallardi, A., Berggren, M., Palazzo, G., Horowitz, G., Ligonzo, T., Torsi, L., 2012. Org. Electron. 13, 638–644.
Deinhammer, R.S., Ho, M., Anderegg, J.W., Porter, M.D., 1994. Langmuir 10, 1306–1313.
Diacci, C., Berto, M., Di Lauro, M., Bianchini, E., Pinti, M., Simon, D.T., Biscarini, F., Bortolotti, C.A., 2017. Biointerphases 12, 05F401.
Fillaud, L., Petenzi, T., Pallu, J., Piro, B., Mattana, G., Noel, V., 2018. Langmuir 34, 3686–3693.
Gan, X., Zhao, H., Quan, X., Zhang, Y., 2016. Electrochim. Acta 190, 480–489.
Gooding, J.J., Hibbert, D.B., Yan, W., 2001. Sensors 1, 75–90.
Kergoat, L., Herlogsson, L., Braga, D., Piro, B., Pham, M.C., Crispin, X., Berggren, M., Horowitz, G., 2010. Adv. Mater. 22, 2565–2569.
Kergoat, L., Herlogsson, L., Piro, B., Pham, M.C., Horowitz, G., Crispin, X., Berggren, M., 2012a. Proc. Nat. Acad. Sci. USA 109, 8394–8399.
Kergoat, L., Piro, B., Berggren, M., Horowitz, G., Pham, M.C., 2012b. Anal. Bioanal. Chem. 402, 1813–1826.
Kozlowski, H., Bal, W., Dyba, M., Kowalik-Jankowska, T., 1999. Coord. Chem. Rev. 184, 319–346.
Liu, G., Nguyen, Q.T., Chow, E., Böcking, T., Hibbert, D.B., Gooding, J.J., 2006. Electroanalysis 18, 1141–1151.
Liu, J., Lu, Y., 2007. Chem. Commun. 4872–4874.
Macchia, E., Manoli, K., Holzer, B., Di Franco, C., Ghittorelli, M., Torricelli, F., Alberga, D., Mangiatordi, G.F., Palazzo, G., Scamarcio, G., Torsi, L., 2018. Nat. Commun. 9,

3223.
Magliulo, M., De Tullio, D., Vikholm-Lundin, I., Albers, W.M., Munter, T., Manoli, K., Palazzo, G., Torsi, L., 2016. Anal. Bioanal. Chem. 408, 3943–3952.
Mulla, M.Y., Tuccori, E., Magliulo, M., Lattanzi, G., Palazzo, G., Persaud, K., Torsi, L., 2015. Nat. Commun. 6, 6010.
Nguyen, T.T.K., Nguyen, T.N., Anquetin, G., Reisberg, S., Noël, V., Mattana, G., Touzeau, J., Barbault, F., Pham, M.C., Piro, B., 2018. Biosens. Bioelectron. 113, 32–38.
Palazzo, G., Tullio, D.D., Magliulo, M., Mallardi, A., Intranuovo, F., Mulla, M.Y., Favia, P., Vikholm-Lundin, I., Torsi, L., 2015. Adv. Mater. 27, 911–916.
Panzer, M.J., Frisbie, C.D., 2006. Adv. Funct. Mater. 16, 1051.
Piro, B., Wang, D., Benaoudia, D., Tibaldi, A., Anquetin, G., Noel, V., Reisberg, S., Mattana, G., Jackson, B., 2017. Biosens. Bioelectron. 92, 215–220.
Porrazzo, R., Bellani, S., Luzio, A., Bertarelli, C., Lanzani, G., Caironi, M., Antognazza, M.R., 2014. APL Mater. 3, 014905.
Sigel, H., Martin, R.B., 1982. Chem. Rev. 82, 385–426.
Suspène, C., Piro, B., Reisberg, S., Pham, M.C., Toss, H., Berggren, M., Yassar, A., Horowitz, G., 2013. J. Mater. Chem. B 1, 2090–2097.
Taniguchi, M., Kawai, T., 2004. Appl. Phys. Lett. 85, 3298.
Thomas, M.S., White, S.P., Dorfman, K.D., Frisbie, C.D., 2018. J. Phys. Chem. Lett. 9, 1335–1339.
Udhayakumari, D., Naha, S., Velmathi, S., 2017. Anal. Methods 9, 552–578.
Wawrzyniak, U.E., Ciosek, P., Zaborowski, M., Liu, G., Gooding, J.J., 2013. Electroanalysis 25, 1461–1471.
White, S.P., Dorfman, K.D., Frisbie, C.D., 2015. Anal. Chem. 87, 1861–1866.
WHO (World Health Organization), 1993. Guidelines for Drinking-Water Quality. Vol. 1. Recommendations, 2nd Ed. Geneva, Switzerland.
Xu, X., Daniel, W.L., Wei, W., Mirkin, C.A., 2010. Small 6, 623–626.
Yao, Z., Yang, Y., Chen, X., Hu, X., Zhang, L., Liu, L., Zhao, Y., Wu, H.C., 2013. Anal. Chem. 85, 5650–5653.
Yang, W., Chow, E., Willett, G.D., Hibbert, D.B., Gooding, J.J., 2003. Analyst 128, 712–718.
Yang, W., Jaramillo, D., Gooding, J.J., Hibbert, D.B., Zhang, R., Willett, G.D., Fisher, K.J., 2001. Chem. Commun. 1982–1983.
Zhu, R., Zhou, G., Tang, F., Tong, C., Wang, Y., Wang, J., 2017. Int. J. Anal. Chem. 2017, 1727126.